TRIGONAL MESHES IN DIFFRACTION TOMOGRAPHY WITH OPTIMUM REGULARIZATION: AN APPLICATION FOR CARBON SEQUESTRATION MONITORING

E.T.F. SANTOS[1], J.M. HARRIS[2], A. BASSREI[3] and J.C. COSTA[4]

[1] *Federal Center of Technological Education of Bahia (CEFET-BA), Salvador, BA, Brazil. eduardot@cefetba.br*
[2] *Department of Geophysics, Stanford University, Stanford, CA, U.S.A.*
[3] *Institute of Physics & Research Center in Geophysics and Geology, Federal University of Bahia, Caixa Postal 1001, 40001-970 Salvador, BA, Brazil.*
[4] *Faculty of Geophysics, Federal University of Pará, Belém, PA, Brazil.*

(Received May 18, 2008; revised version accepted December 30, 2008)

ABSTRACT

Santos, E.T.F., Harris, J.M., Bassrei, A. and Costa, J.C., 2009. Trigonal meshes in diffraction tomography with optimum regularization: an application for carbon sequestration monitoring. *Journal of Seismic Exploration*, 18: 135-156.

Diffraction tomography is an inversion technique that provides the reconstruction of a subsurface velocity field from scattered acoustic field data. High-resolution imaging conventionally requires estimation of a large number of parameters. A trigonal mesh is applied in the study described in this paper, in order to strongly reduce the number of parameters. Thus, instead of a velocity-estimate for each cell in a regular grid, the velocity is estimated only at triangle vertices, which act as control points for the interpolation of velocity field within each triangle. Regularization is required to avoid sharp artifacts due to trigonal elements. A synthetic model is adopted to test the feasibility of the proposed method for reservoir monitoring.

KEY WORDS: inverse problems, diffraction tomography, regularization, trigonal meshes, CO_2 sequestration.

0963-0651/09/$5.00

INTRODUCTION

Tomography techniques have been successfully applied in different areas such as geophysics, medicine and engineering. The underlying principle of tomography is to estimate medium properties based on its projections. In geophysical applications, two main classes of tomographic methods exist: traveltime and waveform tomography. Traveltime tomography uses only traveltimes between different source/receiver pairs in order to estimate the velocity field of a probed region. On the other hand, waveform tomography uses the full waveform to estimate the velocity field. Other medium properties may be estimated as well, e.g., attenuation and velocity anisotropy.

We adopted a particular approach to waveform tomography called diffraction tomography, which uses a first order Born approximation to model the scattered acoustic field. The scattered field is the difference between the measured data and the acoustic field in a known reference velocity field $c^{ref}(\mathbf{r})$. Under this assumption, the scattered field is linearly related to perturbations in the reference velocity field. The reflected pressure field is the input for the inversion procedure, that estimates the two-dimensional velocity field $c^{est}(\mathbf{r})$.

The projection theorem (Devaney, 1984; Harris, 1987; Wu and Toksöz, 1987) provides a direct solution to diffraction tomography. Alternatively, using the matrix formulation (Thompson et al., 1994; Reiter and Rodi, 1996; Rocha Filho et al., 1996), the linear system that models scattering phenomena can be solved using numerical methods (Santos et al., 2006). The main advantages of the matrix formulation are to allow arbitrary survey geometry and the possibility of better conditioning of the inverse problem using *a priori* information. The matrix approach was successfully applied before to diffraction tomography using a regular grid (Santos et al., 2006; Santos and Bassrei, 2007). Its main disadvantage is the cost in terms of computation time when compared with projection methods.

The estimation of the velocity field from measured data using the matrix approach requires the solution of a system. As other inversion techniques applied in geophysics, it is ill-posed. Small perturbations in measured data may result in strong variations in the estimated parameters. It is necessary to introduce additional *a priori* information or constraints to reach realistic solutions. Regularization may provide such information to improve conditioning through smoothness constraints. Tomographic imaging algorithms may require smoothness along vertical direction or more often along the horizontal direction, which might be associated to layering found in many geological situations.

Model parameterization using trigonal meshes has been extensively studied in traveltime tomography (Ajo-Franklin et al., 2006). On the other hand, model

parameterization in diffraction tomography requires a more careful approach, due to the complex nature of the scattering phenomena to be modeled. We propose the use of a linear operator T that maps a trigonal mesh into a regular grid, strongly reducing the number of parameters to be estimated. This mapping approach simplifies the use of trigonal meshes for model parameterization in diffraction tomography. Moreover, conventional techniques applied to a regular grid maps directly into trigonal meshes. Thus, any conventional technique for inversion of a regular grid can be applied to trigonal meshes using this formulation. It does not require the specific modeling of triangular elements scattering. It also makes the proposed approach a framework much more flexible than conventional mesh methods, since it does not require explicit reformulation of regularization and display methods, only requiring an additional linear operator for mapping.

The introduction of regularization in the matrix approach requires a trade-off between data fitness and model smoothness. This balance is achieved by a scalar well-known as the regularization parameter (Hansen, 1992; Hansen, 1998). We tested two approaches to estimate an optimum value for this parameter, the L-curve and the Θ-curve criteria. To solve the regularized diffraction tomography, we apply SVD - Singular Value Decomposition (Lanczos, 1961). This provides an additional possibility to improve the conditioning since the instability of the solution is determined by very small singular values. A complementary approach to regularization is truncate singular values below a certain threshold. The proposed method was applied to a feasibility study of monitoring CO_2 injection in a reservoir using diffraction tomography. The use of trigonal meshes, regularization and optimum strategies for the determination of the regularization parameter were successfully applied to image velocity anomalies produced by CO_2.

LINEAR INVERSION TECHNIQUES

Consider a modeling process where the input of a given system is described by certain parameters contained in vector $\mathbf{m}$ and the output is described as $\mathbf{Am}(= \mathbf{d})$ which is a linear transformation on $\mathbf{m}$. If the vector $\mathbf{d}$ describes the observed output of the system, the problem is to compute the parameters $\mathbf{m}$ in order to minimize in some sense, the difference between the observed $\mathbf{d}$ and the prescribed output of the system $\mathbf{Am}$. If we measure this difference through the norm $\|\bullet\|$, our task is to find the value of $\mathbf{m}$ which minimizes

$$\|\mathbf{Am} - \mathbf{d}\|_2 \ , \tag{1}$$

where the M × N matrix A and the data vector $\mathbf{d}$ with M elements are provided

to the problem. This is called a least-squares problem, which can be formally stated as follows. Considering the basic relationship

$$\mathbf{d} = \mathbf{Am} \quad , \tag{2}$$

we wish to minimize the error using the following objective function:

$$\Phi(\mathbf{m}) = (\mathbf{d} - \mathbf{Am})^{T} \cdot (\mathbf{d} - \mathbf{Am}) \quad . \tag{3}$$

The estimated solution, also called least-squares solution, is

$$\mathbf{m}^{est} = (A^{T}A)^{-1}A^{T}\mathbf{d} \quad . \tag{4}$$

If the matrix $A^{T}A$ is singular we can use the following objective function based on the work of Levenberg (1944) and Marquardt (1963):

$$\Phi(\mathbf{m}) = (\mathbf{d} - \mathbf{Am})^{T} \cdot (\mathbf{d} - \mathbf{Am}) + \lambda \mathbf{m}^{T} \cdot \mathbf{m} \quad .$$

The estimated solution, also called damped least-squares (DLS) solution, is

$$\mathbf{m}^{est} = (A^{T}A + \lambda I)^{-1}A^{T}\mathbf{d} \quad . \tag{6}$$

Generalized inverse (GI) is frequently used in the inversion of geophysical data and its respective solution has the minimum norm. In this case the objective function to be minimized is

$$\Phi(\mathbf{m}) = \mathbf{m}^{T} \cdot \mathbf{m} + \mathbf{t}^{T} \cdot (\mathbf{d} - \mathbf{Am}) \quad , \tag{7}$$

where $\mathbf{t}$ is the vector of Lagrange multipliers. Its minimization yields

$$\mathbf{m}^{est} = A^{T}(AA^{T})^{-1}\mathbf{d} \quad . \tag{8}$$

The concept of GI was developed by Moore and independently by Penrose (1955). Consider an $M \times N$ matrix A. If: (i) $AA^{+}A = A$, (ii) $A^{+}AA^{+} = A^{+}$, (iii) $(AA^{+})^{T} = AA^{+}$, and (iv) $(A^{+}A)^{T} = A^{+}A$, then the $N \times M$ matrix A^{+} is unique. The GI is usually calculated using the singular value decomposition (SVD) (Lanczos, 1961). A rectangular $M \times N$ matrix A with rank k can be decomposed as $A = U\Sigma V^{T}$, where U is the $M \times M$ matrix which contains the orthonormalized eigenvectors of AA^{T}, V is the $N \times N$ matrix which contains the orthonormalized eigenvectors of $A^{T}A$ and Σ is the $M \times N$ diagonal matrix which contains the singular values of A, written in the decreasing order, that is, $\sigma_1 \geq \sigma_2 \geq \ldots \geq \sigma_k$. The GI A^{+} is a $N \times M$ matrix given by $A^{+} = V\Sigma^{+}U^{T}$, where Σ^{+} is the $N \times M$ diagonal matrix which contains the reciprocals of the non-zero singular values of A, so that

$$\Sigma^{+} = \begin{pmatrix} E & 0 & \cdots & 0 \\ 0 & 0 & \cdots & 0 \\ \vdots & \vdots & \ddots & \vdots \\ 0 & 0 & \cdots & 0 \end{pmatrix}, \tag{9}$$

and E is the diagonal square matrix of order k expressed by

$$E = \begin{pmatrix} \sigma_1^{-1} & 0 & \cdots & 0 \\ 0 & \sigma_2^{-1} & \cdots & 0 \\ \vdots & \vdots & \ddots & \vdots \\ 0 & 0 & \cdots & \sigma_k^{-1} \end{pmatrix}. \tag{10}$$

REGULARIZATION BY DERIVATIVE MATRICES

Least-squares solutions very often do not provide good results. In these situations one can apply regularization or smoothing to improve the conditioning of matrix A. This greatly reduces the instability in the least-squares estimate $\mathbf{m}^{est}$, hopefully the resulting smoothed image is not too far from the correct model **m** (Titterington, 1985). The concept of regularization was introduced by Tikhonov in 1963 in order to improve the quality of the inversion. This theory was studied by many researchers, and we use the Twomey (1963) approach. See Bassrei and Rodi (1993) about the names and history in regularization theory. Consider the following objective function:

$$\Phi(\mathbf{m}) = \lambda(D_l\mathbf{m})^T D_l\mathbf{m} + (\mathbf{d} - A\mathbf{m})^T(\mathbf{d} - A\mathbf{m}) \ , \tag{10}$$

where λ is the regularization parameter and D_l is the l-th order derivative matrix. If $\partial\Phi(\mathbf{m})/\partial\mathbf{m} = 0$, then the estimated model is given by

$$\mathbf{m}^{est} = (A^TA + \lambda D_l^T D_l)^{-1} A^T\mathbf{d} \ . \tag{12}$$

Notice that if $\lambda = 0$ we obtain the standard least-squares, and the least-squares is said to be damped if $D_0^T D_0 = I$. If D is the first derivative matrix then the regularization is called to be first order and so on. Each 2D model is scanned line by line to be represented by a single vector. It simplifies the form of the discrete derivative matrix, which resembles a regular pattern. The matrices D_1 [$(M - 1) \times N$] and D_2 [$(M - 2) \times N$] are:

$$D_1 = \begin{pmatrix} -1 & 1 & 0 & 0 & 0 & 0 & 0 & \cdots & 0 \\ 0 & -1 & 1 & 0 & 0 & 0 & 0 & \cdots & 0 \\ \vdots & & & \vdots & \ddots & \vdots & & & \cdots \\ 0 & \cdots & 0 & 0 & 0 & 0 & -1 & 1 & 0 \\ 0 & \cdots & 0 & 0 & 0 & 0 & 0 & -1 & 1 \end{pmatrix} , \quad (13)$$

and

$$D_2 = \begin{pmatrix} 1 & -2 & 1 & 0 & 0 & 0 & 0 & \cdots & 0 \\ 0 & 1 & -2 & 1 & 0 & 0 & 0 & \cdots & 0 \\ \vdots & & & & \ddots & & & & \cdots \\ 0 & \cdots & 0 & 0 & 0 & 1 & -2 & 1 & 0 \\ 0 & \cdots & 0 & 0 & 0 & 0 & 1 & -2 & 1 \end{pmatrix} . \quad (14)$$

DIFFRACTION TOMOGRAPHY MODELING VIA BORN APPROXIMATION

The constant-density acoustic wave equation is given by

$$\nabla^2 U(\mathbf{r},t) = [1/c^2(\mathbf{r})][\partial^2 U(\mathbf{r},t)/\partial t^2] , \quad (15)$$

where $U(\mathbf{r},t)$ is the solution, the total pressure field, and $c(\mathbf{r})$ is the acoustic velocity of the medium. Considering that the solution can be written as $U(\mathbf{r},\omega,t) = e^{-i\omega t}P(\mathbf{r},\omega)$, which represents a harmonic dependence with time, we obtain the Helmholtz equation:

$$[\nabla^2 + k^2]P(\mathbf{r},\omega) = 0 , \quad (16)$$

where the two-dimensional wavenumber is given by $k = k(\mathbf{r},\omega) = \sqrt{(k_x^2 + k_y^2)}$. The conditions for the imaging are that the medium is acoustic and 2D, and the propagation of the incident pressure field is within a limited area $A(\mathbf{r}')$, the background, with constant velocity c_0. The object function is defined as

$$O(\mathbf{r}) = 1 - [c_0^2/c^2(\mathbf{r})] , \quad (17)$$

and represents the perturbation of the velocity in each point in relation to c_0. Redefining the wavenumber as function of $O(\mathbf{r})$, and substituting it in the Helmholtz equation, we obtain

$$[\nabla^2 + k^2]P_S = k_0^2 O(\mathbf{r})[P_O + P_S] \quad , \tag{18}$$

where P_O is the incident pressure field, P_S is the scattered pressure field and k_0 is the homogeneous wavenumber, given by $k_0 = \omega/c_0$. Eq. (18) is a differential equation with the following integral solution, known as Lippmann-Schwinger equation (Lo and Inderwiesen, 1994):

$$P_S(\mathbf{r}) = -k_0^2 \int_{A(\mathbf{r}')} O(\mathbf{r}')G(\mathbf{r}|\mathbf{r}')[P_O(\mathbf{r}') + P_S(\mathbf{r}')]d\mathbf{r}' \quad . \tag{19}$$

In the inverse scattering procedure, we consider that the scattered pressure field is known at the domain boundary, the object function is the unknown function, and the integral above becomes an integral equation. The equation (19) is non-linear and its linearization is achieved, for example, via the first order Born approximation, which is only valid for the weak scattering of the incident pressure field. The total pressure field is $P_T(\mathbf{r}) = P_O(\mathbf{r}) + P_S(\mathbf{r})$ and $P_S(\mathbf{r}) \ll P_O(\mathbf{r})$, so that we have $P_T(\mathbf{r}) = P_O(\mathbf{r})$. Thus we obtain a linear relation between $O(\mathbf{r})$ and $P_S(\mathbf{r})$:

$$P_S(\mathbf{r}) = -k_0^2 \int_{A(\mathbf{r}')} O(\mathbf{r}')G(\mathbf{r}|\mathbf{r}')P_O(\mathbf{r}')d\mathbf{r}' \quad . \tag{20}$$

We represent the incident pressure field by a source in $\mathbf{r}_S$ through Green's function:

$$P_O(\mathbf{r}') = G(\mathbf{r}_S|\mathbf{r}') \quad , \tag{21}$$

and the scattered pressure field in $A(\mathbf{r})$ is registered by a receptor in $\mathbf{r}_G$:

$$P_S(\mathbf{r}_S,\mathbf{r}_G) = -k_0^2 \int_{A(\mathbf{r}')} O(\mathbf{r}')G(\mathbf{r}_G|\mathbf{r}')\, G(\mathbf{r}_S|\mathbf{r}')\, d\mathbf{r}' \quad . \tag{22}$$

The discretization of the above expression leads to the linear relation $\mathbf{d} = \mathbf{Am}$, which has to be inverted in order to recover $O(\mathbf{r})$. In this work, the inversion is performed using SVD with regularization, which we described earlier.

TRIGONAL MESHES

We propose the use of trigonal meshes for diffraction tomography in order to reduce the number of parameters to be estimated. However, we also want to keep the simple formulation of the tomographic matrix and regularization for

conventional regular grids. Thus, we derived a different formulation for the use of trigonal meshes that allows mapping between triangle vertices and a regular grid. This approach can be used as a general framework to solve linear inverse problems for different areas using triangles instead of rectangular cells as basic elements, with minimal impact on original problem formulation.

The key concept is to describe each cell of a regular grid as a linear combination of control node-values at triangle vertices, considering the respective triangle that covers each region of regular grid. Thus, a linear operator T may be explicitly defined to map the control nodes of a trigonal mesh into any regular grid. The algorithm that computes matrix T has the following steps:

For each mesh triangle:

- identify its three vertices to compute three respective vertex weights based on the relative position of interior cells of this triangle;
- compute three weights for each node of the regular grid within the current triangle using barycentric coordinates interpolation;
- store these weights into the matrix T which allows to compute each node value of the regular grid as a linear combination of values at the nodes of the trigonal mesh.

The interpolation using barycentric coordinates is based on the areas of three imaginary triangles formed by lines between triangle vertices and an interior point as can be seen in Fig. 1 (Bottema, 1982). These three areas are used as a measurement of influence of each control node vertex onto an interior point, resulting in three respective weights for each discretized interior point. Considering v_1, v_2 and v_3 as the control values at respective positions $\mathbf{r}_1$, $\mathbf{r}_2$ and $\mathbf{r}_3$ corresponding to vertexes of each triangle, the weights for each interior point at position $\mathbf{r}$ using barycentric interpolation are given by:

$$w_1(\mathbf{r}) = [(\mathbf{r} - \mathbf{r}_2) \times (\mathbf{r}_3 - \mathbf{r}_2)\cdot\mathbf{e}_3]/[(\mathbf{r}_1 - \mathbf{r}_2) \times (\mathbf{r}_3 - \mathbf{r}_2)\cdot\mathbf{e}_3] \quad , \qquad (23)$$

$$w_2(\mathbf{r}) = [(\mathbf{r} - \mathbf{r}_1) \times (\mathbf{r}_3 - \mathbf{r}_1)\cdot\mathbf{e}_3]/[(\mathbf{r}_2 - \mathbf{r}_1) \times (\mathbf{r}_3 - \mathbf{r}_1)\cdot\mathbf{e}_3] \quad , \qquad (24)$$

and

$$w_3(\mathbf{r}) = [(\mathbf{r} - \mathbf{r}_1) \times (\mathbf{r}_2 - \mathbf{r}_1)\cdot\mathbf{e}_3]/[(\mathbf{r}_3 - \mathbf{r}_1) \times (\mathbf{r}_2 - \mathbf{r}_1)\cdot\mathbf{e}_3] \quad , \qquad (25)$$

where $\mathbf{e}_3$ is the unitary vector (0,0,1). This leads to the following expression that maps node-control values from a trigonal mesh onto a regular grid cell value

$O(\mathbf{r})$ for each triangle:

$$O(\mathbf{r}) = \sum_{i=1}^{3} w_i(\mathbf{r}) v_i(\mathbf{r}_i) \quad . \tag{26}$$

The matrix T performs the mapping of a trigonal mesh to an arbitrary point $\mathbf{r}$ using respective triangles that covers its different regions. Thus, node-control values at triangle vertices can be mapped into a regular grid using the following forward mapping expression:

$$\mathbf{o} = \mathrm{T}\mathbf{v} \quad . \tag{27}$$

The object function $O(\mathbf{r})$ is discretized into regular grid cell values vector $\mathbf{o}$. From a simple regular grid formulation for linear problems:

$$\mathbf{p} = \mathrm{W}\mathbf{o} \quad , \tag{28}$$

where $\mathbf{p}$ is the data vector and $\mathbf{o}$ is the parameter vector, one may use the following expression for trigonal meshes:

$$\mathbf{p} = \mathrm{WT}\mathbf{v} \quad . \tag{29}$$

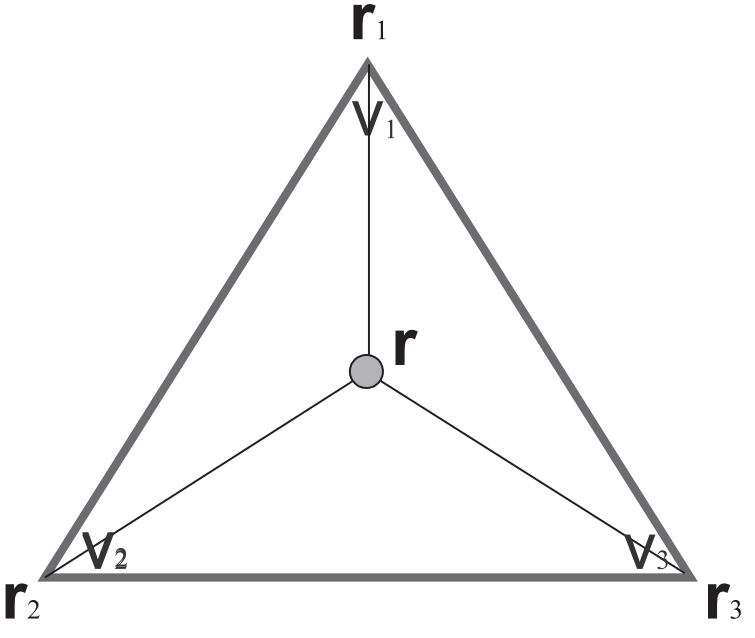

Fig. 1. Structure of the trigonal element.

For linear inverse problems, this expression can be applied to estimate trigonal mesh control node values from data vector:

$$\mathbf{v} = (\mathrm{WT})^{+}\mathbf{p} \quad ,$$

where the superscripted plus symbol means pseudo-inverse computed using SVD. The same expression can be rewritten for the least-squares formulation:

$$\mathbf{v} = [(\mathrm{WT})^{\mathrm{T}}(\mathrm{WT})]^{+}(\mathrm{WT})^{\mathrm{T}}\mathbf{p} \quad . \tag{30}$$

The following equivalent regularized system can be obtained:

$$\begin{pmatrix} \mathrm{W} \\ \\ \mathrm{D} \end{pmatrix} \mathrm{T}\mathbf{v} = \begin{pmatrix} \mathbf{p} \\ \\ 0 \end{pmatrix} . \tag{31}$$

where D is a numerical first-derivative matrix. After the parameter estimation, the resulting trigonal mesh control values can be easily displayed as a regular grid using forward mapping of linear operator T, as described earlier.

NUMERICAL SIMULATION

We considered a true model with 50 × 50 = 2,500 cells, which can be seen in Fig. 2. Each cell has the size of 3 × 3 m. The acquisition geometry was the conventional seismic reflection survey, where sources and receivers are located at the top of the model. The background medium velocity is 4,000 m/s. There is a negative velocity contrast caused by CO_2 injection that causes a minus 2% contrast. This model represents injected CO_2 at bottom level which escaped through a leak due to a fault, forming an upper plume, an important situation to be detected for safety assessment. In each configuration there are 15 sources and 15 receivers, in such a way that the data set has 225 data points. But since we separated the complex numbers into real and imaginary parts, we have in fact 450 points of information, making the tomographic matrix rectangular (450 × 2,500). Since there are more parameters to be estimated than available information, this matrix is underdetermined and would not provide a reasonable parameter estimation for such resolution. We applied the proposed trigonal mesh mapping to reduce the number of parameters to be estimated. Fig. 3 shows an ideal estimated model using triangles for forward mapping from the true model. This estimate is used as reference for comparison purposes, since it is the best possible reconstruction of the true model shown in Fig. 2, using a regular trigonal mesh. The meshes were generated using function calls to a Matlab toolbox called Distmesh (Persson and Strang, 2004).

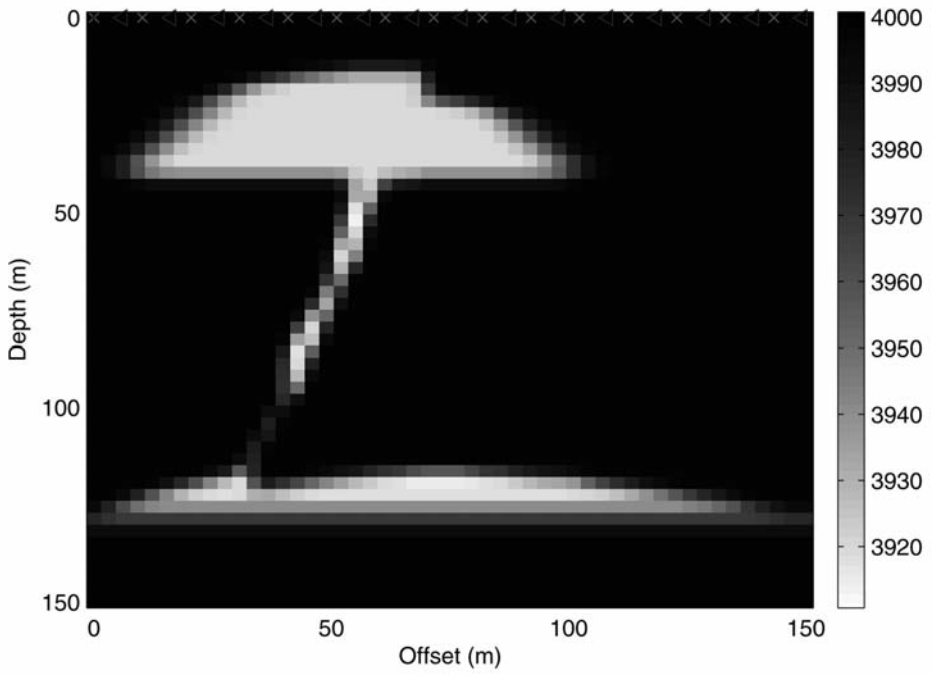

Fig. 2. True model and the seismic reflection profile acquisition geometry.

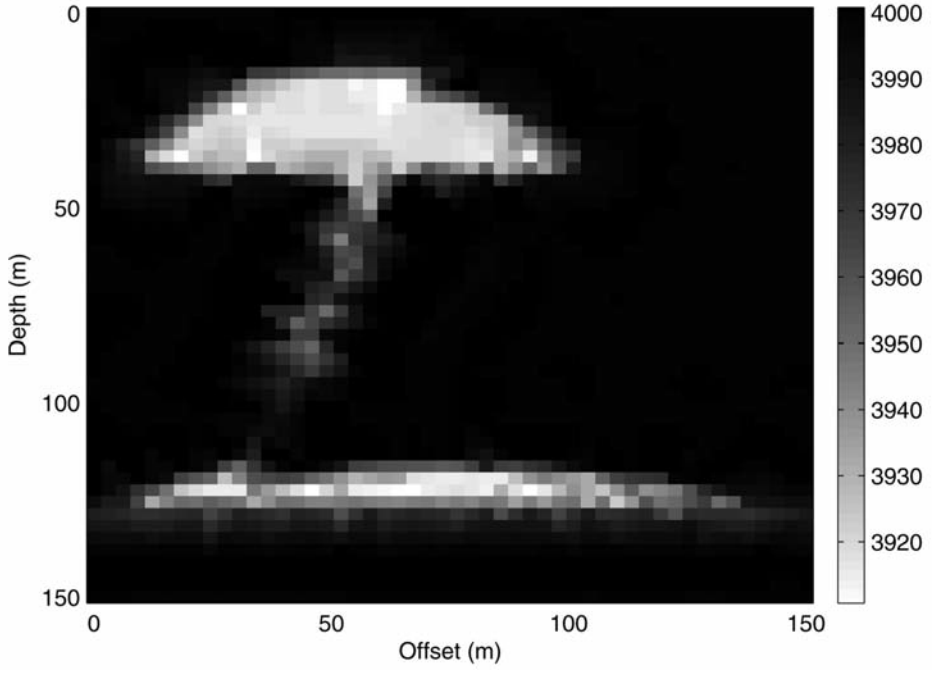

Fig. 3. Trigonal mapping of the true model (reference true model).

Fig. 4 shows a regular trigonal mesh with 199 vertices that act as control nodes, strongly reducing the number of parameters to be estimated. Using the proposed forward mapping for trigonal meshes, the tomographic matrix dimensions now become 450 × 199, which leads to an overdetermined system, allowing a more feasible parameter estimation using diffraction tomography. Fig. 5 shows the resulting noise-free inversion for this regular trigonal mesh, using second order regularization and $\lambda = 0.10$. The choice of λ was based on a trial and error procedure. The leakage is well-delineated although one can notice a light blur in the right region of the model, around the coordinates (x,y) = (120,75) meters.

In order to evaluate the regular trigonal mesh approach we also employed the standard methodology for parametrization, which is the application of a regular rectangular mesh. Fig. 6 shows the estimated model where one can see many artifacts in the region $120 < x < 150$ meters for the whole depth and the plume itself is not well defined. This result was obtained using second order regularization ($\lambda = 0.15$) and with noise-free data. Also with regular rectangular meshes one can have an overdetermined system. For example, using

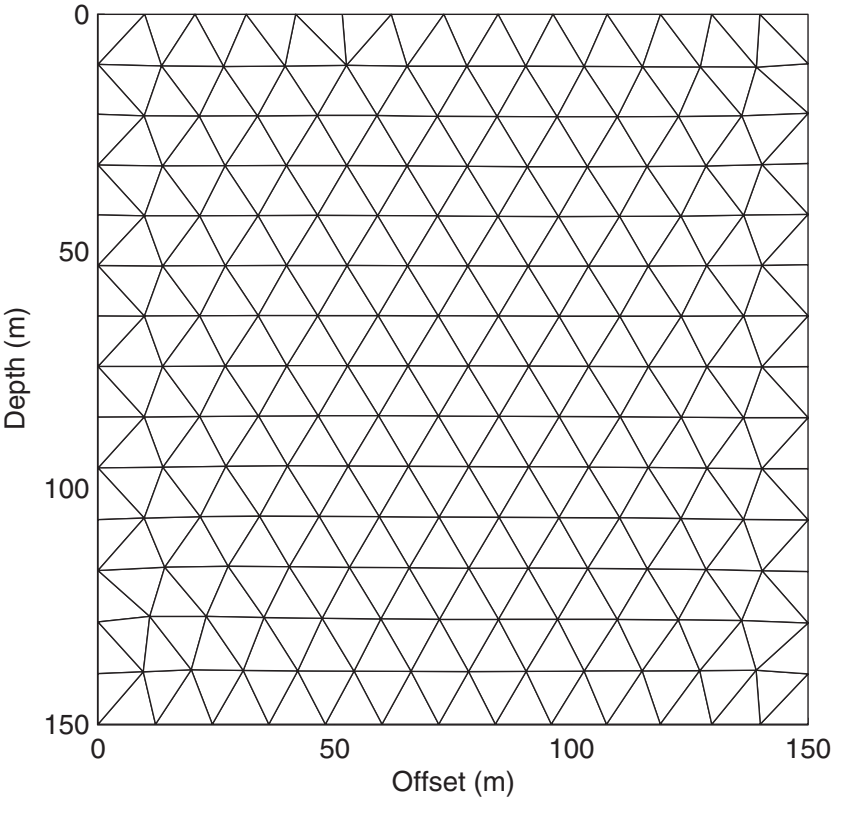

Fig. 4. Regular trigonal mesh using 199 vertices.

400 rectangles (20 × 20), which means a model with much less resolution, but with the same number of data points, we obtained the estimated model that can be seen in Fig. 7. Now there are less artifacts but the plume itself lost its structure. We can see that these two images (Figs. 6 and 7) are very different. This is due to a lack of resolution in the model parameters. Comparing the result with the regular trigonal mesh (Fig. 5) with the underdetermined regular rectangular one (Fig. 6), we verify that the image in Fig. 5 defines much better the heterogeneity edges and displays much less artifacts.

An adaptive mesh is shown in Fig. 8, refining the mesh at the contours of negative contrast, resulting into 351 vertices, which still leads to an overdetermined system. This adaptive mesh can be generated based on reservoir flow simulation prediction. It is obtained by generation of smaller triangles at regions with fast velocity variations and bigger triangles at nearly homogeneous regions. The velocity variation is measured by the numerical spatial gradient of velocity and mapped into finer or coarser meshes depending on respective region characteristics. Fig. 9 shows, for this new mesh, the noise-free inversion without regularization. From this result, the need for some regularization procedure is obvious. Fig. 10 shows the noise-free inversion obtained for this adaptive mesh, using second order regularization with $\lambda = 0.10$, again based on a trial and error procedure. The leakage is well delineated, although there is a light blur around (x,y) = (120, 75) meters.

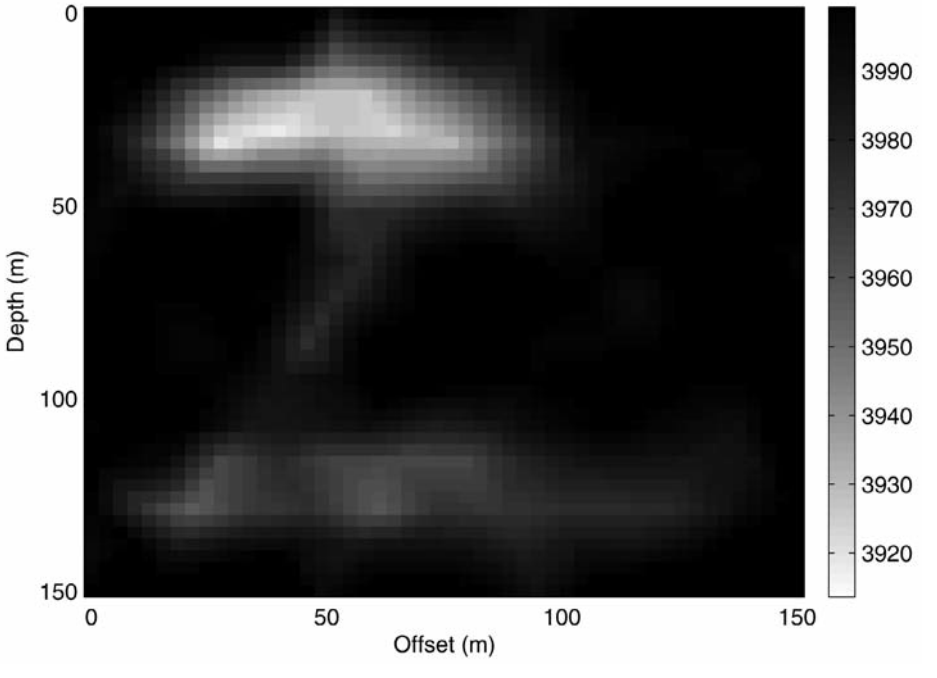

Fig. 5. Estimated noise-free model with second order regularization ($\lambda = 0.15$) using a regular trigonal mesh.

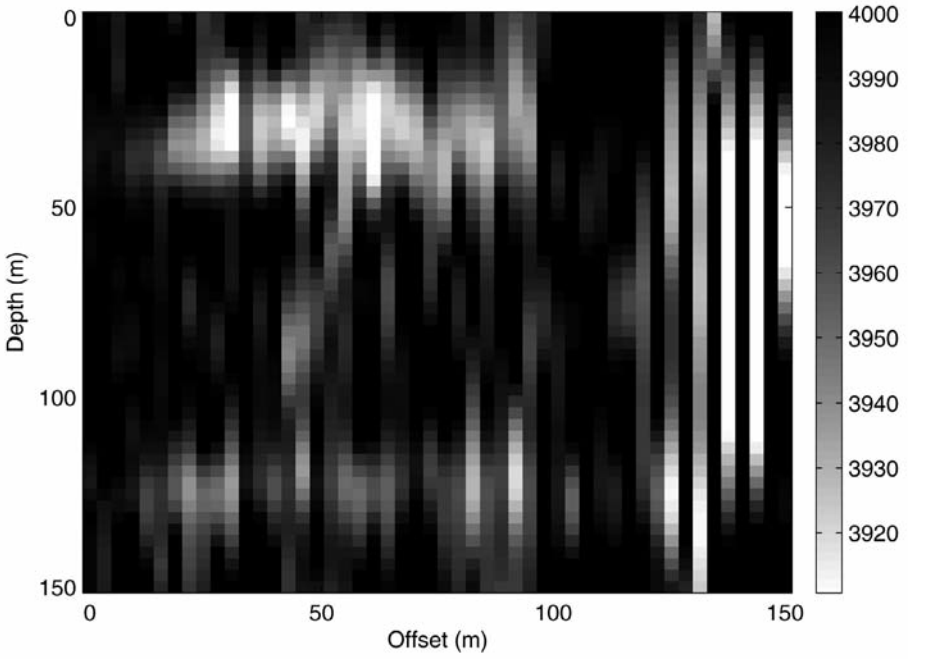

Fig. 6. Estimated noise-free model with second order regularization ($\lambda = 0.15$) using a regular rectangular mesh with 2,500 rectangles.

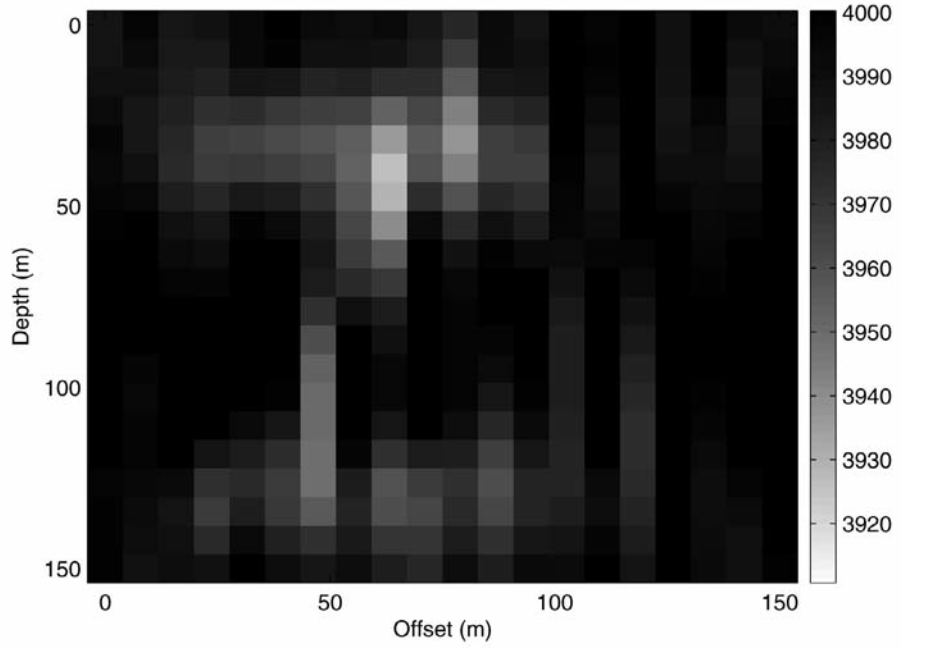

Fig. 7. Estimated noise-free model with second order regularization ($\lambda = 0.15$) using a regular rectangular mesh with 2,500 rectangles.

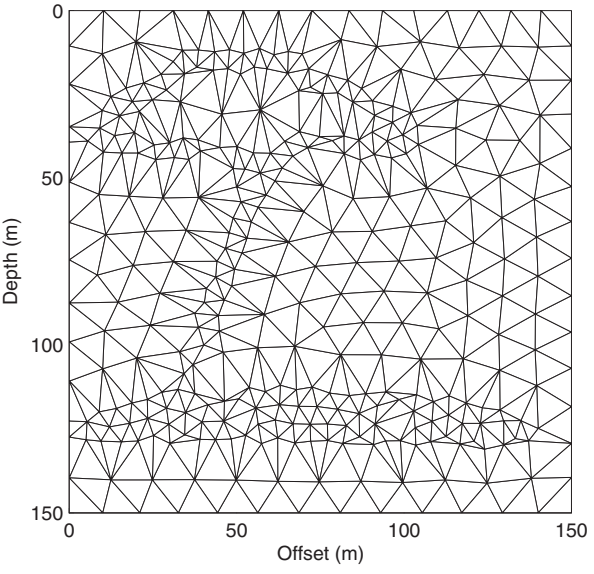

Fig. 8. Adaptive trigonal mesh using 351 vertices.

In order to increase the effectiveness of the regularization technique, we used the L-curve for the search of the optimum regularization parameter. An illustrative L-curve is shown in Fig. 11. The error between the calculated data and the observed one is represented in the horizontal axis, that is, $\|\mathbf{e}\| = \|\mathbf{d}^{cal} - \mathbf{d}^{obs}\| = \|\mathbf{A}\mathbf{m}^{est} - \mathbf{d}^{obs}\|$. In the vertical axis one has the derivative matrix multiplied by the estimated solution. In other words, that is the amount of regularization and it is expressed by $\|\mathbf{D}_n\mathbf{m}^{est}\|$, where n is the regularization order. The regularization parameter is expressed by λ, and for each estimated solution $\mathbf{m}^{est}$ there is a different λ. The L-curve knee represents a trade-off between smoother solutions with higher errors and rougher solutions with smaller errors. The knee detection at the L-curve is an heuristic criterion to select the most appropriate solution. A number of different definitions have been proposed for the best estimation of the L-curve corner (Belge et al., 2002; Kilmer and O'Leary, 2001; Hansen, 1992, 1998). Considering this curve approximately L-shaped, one can find its knee searching the maximum curvature point (Hansen, 1992; Hansen and O'Leary, 1993). Although, secondary inflexions may occur, which may result in the wrong detection of the best regularization parameter. Thus, the automatic method of knee detection may lead sometimes to inadequate regularization parameters. Due to this problem, sometimes it is necessary to select the best regularization parameter by visual inspection of the L-curve and a manual detection of its knee. Belge at al. (2002) adopted the point closest to the origin of L-curve graph as an estimation of the L-curve corner. It works fine when the curve is clearly L-shaped, but it may fail when the inflexion at knee significantly differs from a straight angle because another points outside knee may be closer to the origin.

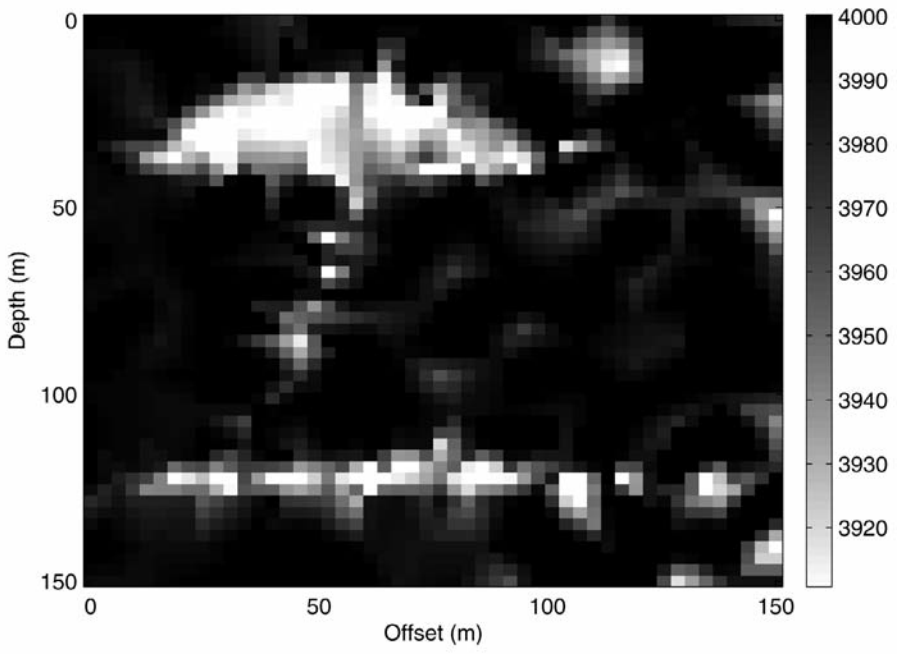

Fig. 9. Estimated noise-free model without regularization using an adaptive trigonal mesh.

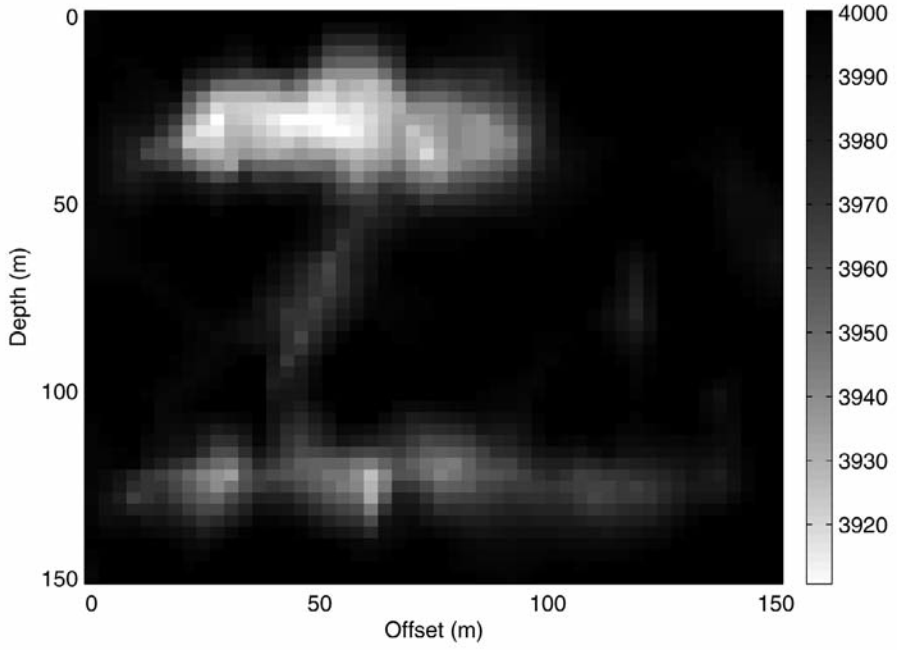

Fig. 10. Estimated noise-free model with second order regularization ($\lambda = 0.10$) using an adaptive trigonal mesh.

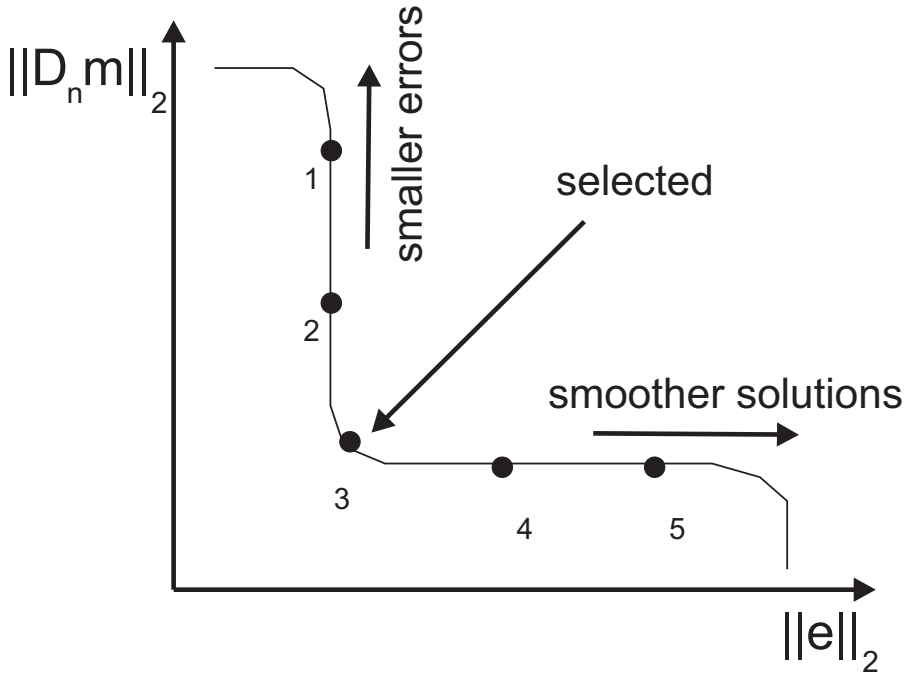

Fig. 11. Illustrative L-curve: the curve inflexion provides the optimum regularization parameter.

The L-curve for this example using second order regularization can be seen in Fig. 12. We added 10% peak-to-peak Gaussian noise in the values of the scattered pressure field. This is a typical example where the L-curve does not resemble the shape of letter "L". By visual inspection we selected the best regularization parameter as $\lambda = 0.06064$. Using this λ we calculated the reconstructed tomogram displayed in Fig. 13. The leakage is again well delineated, although there is a light blur around (x,y) = (120, 75) meters.

We also used the Θ-curve, proposed by Santos et al. (2006) and Santos and Bassrei (2007). It is based on a curve representing the cosine of angles between adjacent segments of the L-curve discrete representation, as can be seen in Fig. 14. Where the curve is locally straight, the angle tends to zero, leading the cosine of this angle to one. Near the L-curve corner, the angle tends to be greater than its neighbors, leading the cosine to values below one. Thus, smaller values of cosine are associated with inflexions of the curve, which lead us to inspect the minima of the Θ-curve in order to find the corner of L-curve and consequently the best regularization parameter. The method developed to select the best regularization parameter is based on the detection of the first local minimum of the Θ-curve. This minimum is automatically detected where the first derivative is close to zero and the second derivative is positive, adopting thresholds due to the discretization and arithmetic computer precision. Thus, the

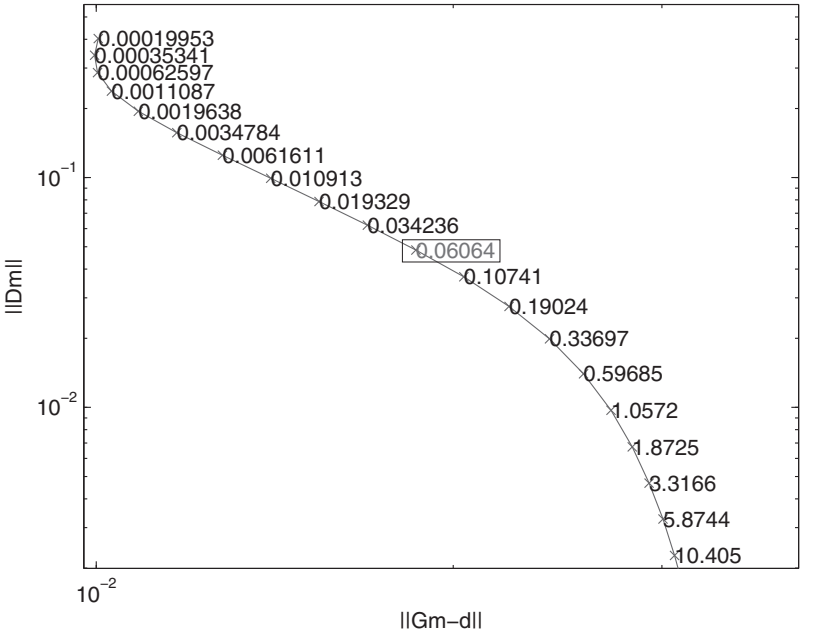

Fig. 12. L-curve for second order regularization and 10% peak-to-peak noise. The numbers represent different values for λ.

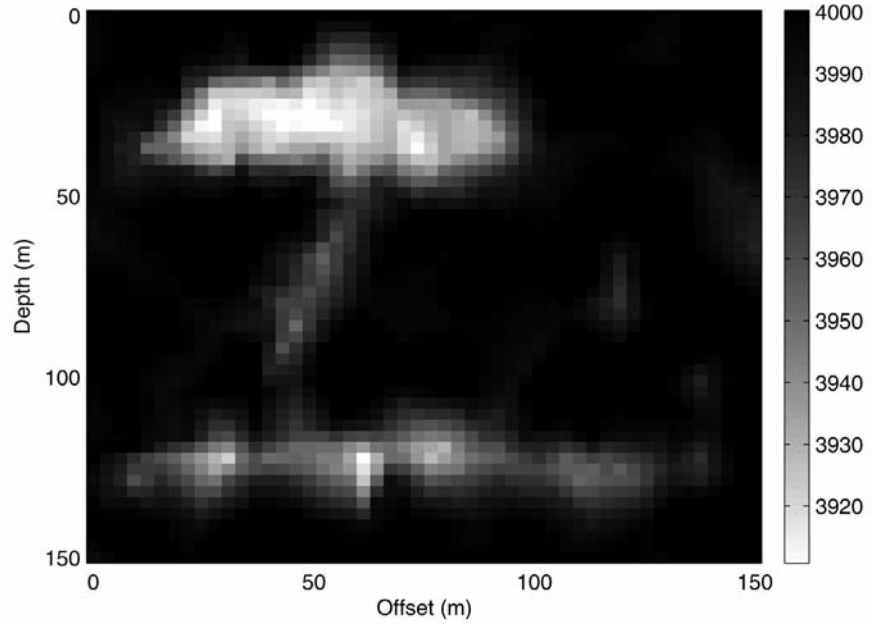

Fig. 13. Estimated model from 10% noise-data with second order regularization using an adaptive trigonal mesh. Optimum regularization parameter (λ = 0.06064) provided from the L-curve shown in Fig. 12.

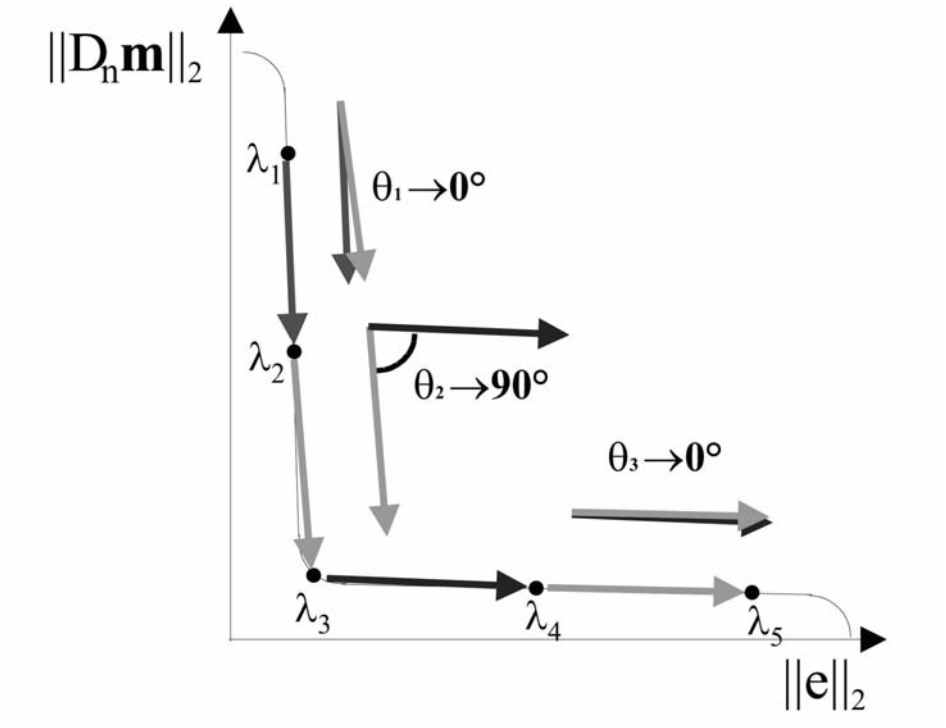

Fig. 14. Illustrative scheme for the construction of Θ-curve.

first occurrence of minimum at the Θ-curve is associated with the corner of L-curve, which is related to the optimal regularization parameter. Further inflexions of the L-curve are associated to local minima of the Θ-curve and may also be inspected when the L-curve is not "L-shaped". This feature of the Θ-curve is important to improve the robust detection of the regularization parameter. In general one can conclude that the Θ-curve automatic criterion is more robust than the search for maximum curvature of the L-curve (Santos et al., 2006; Santos and Bassrei, 2007).

The Θ-curve for the leakage example using second order regularization is shown in Fig. 15, where it can be seen that the optimum regularization parameter is $\lambda = 0.10741$. This is the case when the L-curve is not "L-shaped". The first minimum is the global one and the second, which was selected, is the local one. Again we added 10% peak-to-peak Gaussian noise in the values of the scattered pressure field. Using this λ we reconstructed the tomogram displayed in Fig. 16. This image is very close to the tomograms shown in Fig. 10 and Fig. 13.The advantage here is the fact that the Θ-curve provides the optimum parameter in a more visible form when compared to the L-curve.

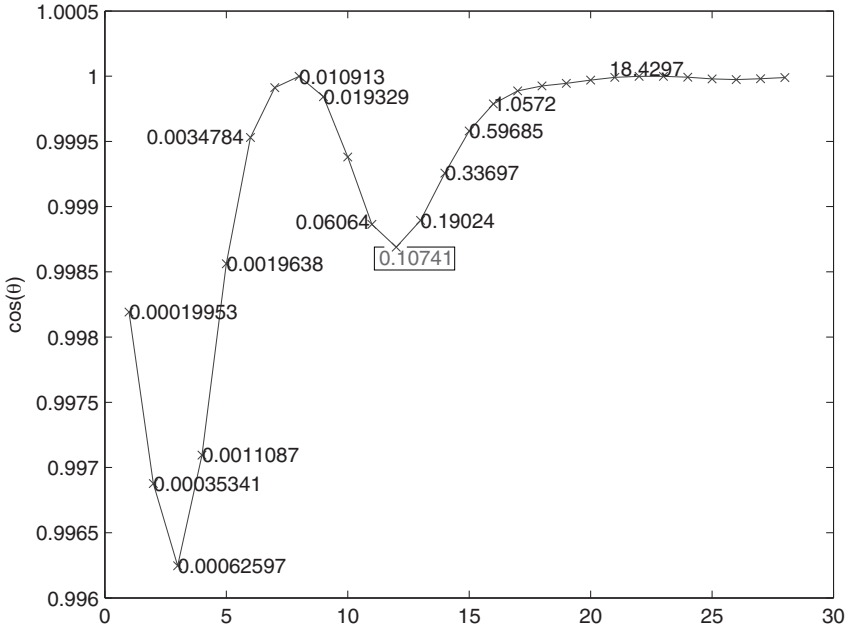

Fig. 15. Θ-curve for second order regularization and 10% peak-to-peak noise. The numbers represent different values for λ.

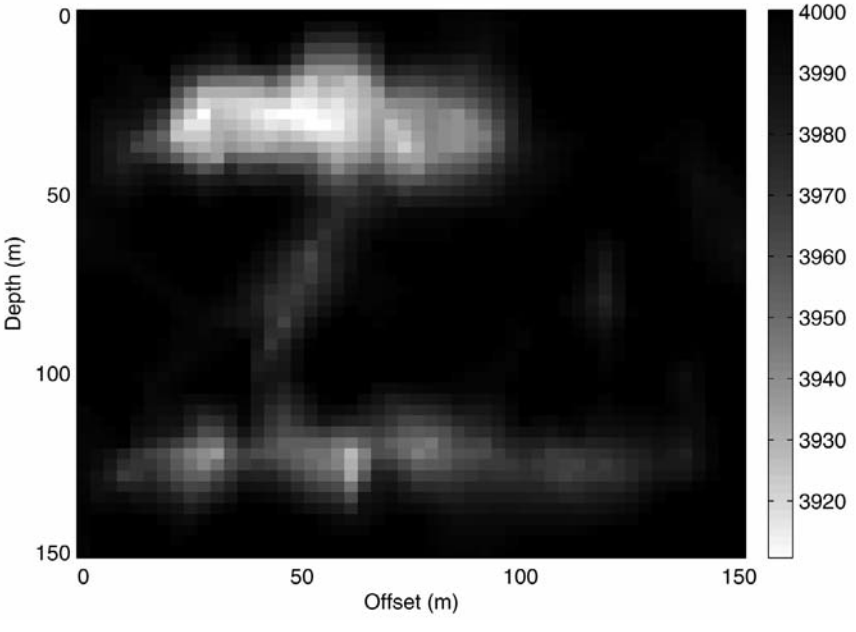

Fig. 16. Estimated model from 10% noise-data with second order regularization using an adaptive trigonal mesh. Optimum regularization parameter (λ = 0.10741) provided from the Θ-curve shown in Fig. 15.

The adaptive trigonal mesh has as its main advantage a higher level of detail close to the contours of injected CO_2. Since it uses different sizes of triangles causing different uncertainties in the results, some stretched triangles between coarse and fine mesh regions may introduce artifacts that can be minimized through the use of regularization.

CONCLUSIONS

Trigonal meshes strongly reduce the number of parameters to be estimated. Problems that were originally underdetermined can be reformulated as overdetermined without the drastic decrease of resolution required for regular grids under similar circumstances. We show through a synthetic model inversion how trigonal meshes reduce the number of parameters and how a conventional regular grid method can be easily adapted to use triangular elements instead of uniform sized cells. This forward mapping can be used as a general framework for improvement of many existing regular grid algorithms minimizing the impact onto the original formulation. The proposed method also provides a simple inverse mapping for visualization purposes of a trigonal mesh. The synthetic model was properly recovered using a small survey for regularized diffraction tomography applied to a regular and an adaptive trigonal mesh. Both meshing approaches successfully detected the target, an important feature for reservoir monitoring.

ACKNOWLEDGMENTS

The authors would like to acknowledge Jaime Urban for the original CO_2 model adapted in this work. We also would like to acknowledge Stanford's University Global Climate and Energy Project, the Smart Fields industrial affiliates, and the Center for Computational Earth and Environmental Science. A. Bassrei would like to thank CNPq for the projects 484.239/2006-6 (Universal Edict MCT/CNPq 02/2006) and 308.875/2007-9 (research fellowship).

REFERENCES

Ajo-Franklin, J.B., Urban, J.A. and Harris, J.M., 2006. Using resolution-constrained adaptive meshes for traveltime tomography. J. Seismic Explor., 14: 371-392.

Bassrei, A. and Rodi, W.L., 1993. Regularization and inversion of linear geophysical data. 3rd Internat. Congr. Brazil. Geophys. Soc., Rio de Janeiro, Brazil, I: 111-116.

Belge, M., Kilmer, M.E. and Miller, E.L., 2002. Efficient determination of multiple regularization parameters in a generalized L-curve framework. Inverse Problems, 18: 1161-1183.

Bottema, O., 1982. On the area of a triangle in barycentric coordinates. Crux Mathematic., 8: 228-231.

Devaney, A.J., 1984. Geophysical diffraction tomography.Inst. Electr. Electron. Engin. Transact. Geosci. Remote Sens., 22: 3-13.

Hansen, P.C., 1992. Analysis of discrete ill-posed problems by means of the l-curve. Soc. Industr. Appl. Mathemat. Rev., 34: 561-580.

Hansen, P.C., 1998. Rank-Deficient and Discrete Ill-Posed Problems. Soc. Industr. Appl. Mathemat, Philadelphia.

Hansen, P.C. and O'Leary, D.P., 1993. The use of the L-curve in the regularization of discrete ill-posed problems. Soc. Industr. Appl. Mathemat. J. Scientif. Computat., 14: 1487-1503.

Harris, J.M., 1987. Diffraction tomography with discrete arrays of sources and receivers. Inst. Electr. Electron. Engin. Transact. Geosci. Remote Sens., 25: 448-455.

Kilmer, M.E., O'Leary, D.P., 2001. Choosing Regularization Parameters in Iterative methods for ill-posed problems. Soc. Industr. Appl. Mathemat. J. Matrix Analys. Applic., 22: 1204-1221.

Lanczos, C., 1961. Linear Differential Operators. Van Nostrand, London.

Levenberg, K., 1944. A method for the solution of certain non-linear problems in least-squares. Quart. Appl. Mathemat., 2: 164-168.

Lo, T.-W. and Inderwiesen, P.L., 1994. Fundamentals of Seismic Tomography. Geophysical Monograph Series, SEG, Tulsa, OK.

Marquardt, D.W., 1963. An algorithm for least-squares of nonlinear parameters. J. Soc. Industr. Appl. Mathemat., 11: 431-441.

Penrose, R., 1955. A generalized inverse for matrices. Proc. Cambridge Philosoph. Soc., 51: 406-413.

Persson, P.-O. and Strang, G., 2004. A simple mesh generator in MATLAB. Soc. Industr. Appl. Mathemat. Rev., 46: 329-345.

Reiter, T.D. and Rodi, W., 1996. Nonlinear waveform tomography applied to crosshole seismic data. Geophysics, 61: 902-913.

Rocha Filho, A.A., Harris, J.M. and Bassrei, A., 1996. A simple matrix formulation diffraction tomography algorithm. 39th Congr. Brasil. Geol., Salvador, BA, Brasil, 2: 312-315.

Santos, E.T.F., Bassrei, A. and Costa, J., 2006. Evaluation of L-curve and Θ-curve approaches for the selection of regularization parameter in anisotropic traveltime tomography. J. Seismic Explor., 15: 245-272.

Santos, E.T.F. and Bassrei, A., 2007. L- and Θ-curve approaches for the selection of regularization parameter in geophysical diffraction tomography. Comput. Geosci., 33: 618-629.

Thompson, D.R., Rodi, W. and Toksöz, M.N., 1994. Nonlinear seismic diffraction tomography using minimum structure constraints. J. Acoust. Soc. Am., 95: 324-330.

Titterington, D.M., 1985. General structure of regularization procedures in image reconstruction. Astron. Astrophys., 144: 381-387.

Twomey, S., 1963. On the numerical solution of Fredholm integral equations of the first kind by the inversion of the linear system produced by quadrature. J. Assoc. Comput. Mach., 10: 97-101.

Wu, R.-S. and Toksöz, M.N., 1987. Diffraction tomography and multisource holography applied to seismic imaging. Geophysics, 52: 11-25.